Supplementary: A new method for the retrieval of the equivalent refractive index of atmospheric aerosols

S. Vratolis☆[1,2], P. Fetfatzis[1], A. Argyrouli[2], A. Papayannis[2], D. Müller[5], I. Veselovskii[10,11], A. Bougiatioti[2,3,4], A. Nenes[4,6,7,8], E. Remoundaki[9], E. Diapouli[1], M. Manousakas[1], M. Mylonaki[2], K. Eleftheriadis[1]

[1]ERL, Institute of Nuclear & Radiological Sciences & Technology, Energy & Safety, National Centre of Scientific Research Demokritos, 15310 Ag. Paraskevi, Attiki, Greece
[2]Laser Remote Sensing Unit, Physics Department, School of Applied Mathematics and Physical Sciences, National Technical University of Athens (NTUA), 15780 Zografou, Greece
[3]ECPL, Department of Chemistry, University of Crete, Voutes, 71003 Heraklion, Greece
[4]School of Earth & Atmospheric Sciences, Georgia Institute of Technology, Atlanta, GA 30332, USA.
[5]School of Physics, Astronomy and Mathematics, University of Hertfordshire, Herts AL 10 9AB, UK
[6]ICE-HT, Foundation for Research and Technology, Hellas, 26504 Patras, Greece
[7]Institute of Environmental Research and Sustainable Development, National Observatory of Athens, Athens, Greece
[8]School of Chemical & Biomolecular Engineering, Georgia Institute of Technology, Atlanta 30332, GA, USA
[9]Laboratory of Environmental Science and Engineering, School of Mining and Metallurgical Engineering, National Technical University of Athens, 15780 Zografou, Greece
[10]Physics Instrumentation Center of GPI, Troitsk, Moscow, Russia
[11]Joint Center for Earth Systems Technology, UMBC, Baltimore, USA

Supplementary: Method Evaluation - Calibration Procedure

Figure S1 displays the layout during the experiments. The aerosol particle generator used was a TOPAS ATM 220, which provided a high number of aerosol particles in the overlapping range of the two instruments. The calibration was carried out at DEM-GAW station and the instruments were sampling from their station inlet line. The generated aerosol was brought to a mixing chamber, where it was mixed with dry, particle free air. Mixing ratios varied, depending on the final concentration needed for the calibration. The aerosol was then lead to the inlet line, into a vertical nafion dryer with a length of 60 cm and internal diameter approximately 1 cm, and was subsequently distributed to the two instruments. During the experiments, inlet flow had an RH equal to 15 ± 9%, while temperature was 22 ± 8 °C.

PSL spheres with nominal diameters of 262 and 490 nm were diluted in MilliQ water. A bimodal NSD for both instruments was expected, as both instruments are calibrated with this compound.

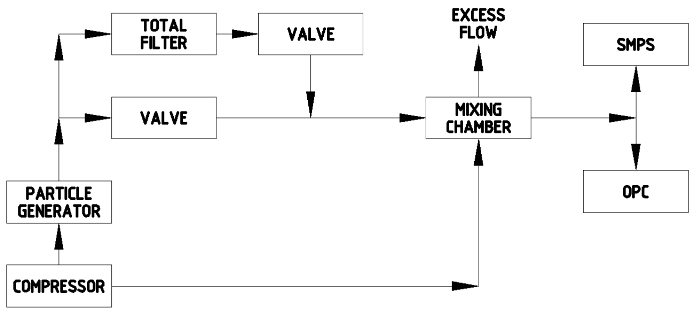

Figure S1: Calibration of SMPS-OPC ERI setup.

As denoted in Figure S2, the OPC has a peak at 430 nm (corresponding to 490 nm PSL), while we cannot be sure about the peak for the 262 nm PSL. The lognormal fit based on the three first size bins of the OPC overestimates the PSL concentration dramatically. This is probably due to the fact that the boundaries of the first size bin of the OPC are not correctly attributed, while in these size bins aerosol particles with smaller sizes than the nominal minimum are counted. Therefore, we have a very steep

☆Corresponding Author
Email address: vratolis@ipta.demokritos.gr (S. Vratolis)

slope of the lognormal distribution fitted to the data, thus the error in the number concentration predicted is very large.

In order to correct for the sizing error, we consider the OPC measurement principal. It can be described as follows: Air containing particles is drawn through an illuminated volume, where light scattered by single particles is sensed and converted to an electrical signal, whose pulse height is analyzed. The pulse height is used to infer particle size. The measurement of many particles results in a size distribution. Particle concentration in every size bin is determined from total counts in that size range. An error in the electrical signal pulse height would result in erroneous sizing of the aerosol particle. We need to know the relation of this error in the working size range of the instrument.

The simplest assumption would be that the error is related to the amplification of the scattering signal, therefore the scattering signal expected should be divided by a constant factor. To investigate that, we plot S_{sca} calculated by Mie theory and given particle size, for the OPC geometry, assuming homogeneous aerosol particles with an RI equal to 1.585. According to the PSL experiment, 490 nm particles are detected as 430 nm. We need to adjust S_{sca} so that the signal that corresponds to a particle with a diameter of 430 nm, will now correspond to a 490 nm particle. According to Figure S2 (supplementary), if we divide S_{sca} by a factor of 1.5, we have a signal curve that corrects the error observed at the PSL experiment.

The size correction for the OPC is incorporated into the optimal solution algorithm by assuming it is a constant factor in the common size range of the two instruments.

SMPS sizes the 490 nm PSL correctly and slightly underestimates the 262 nm PSL.

If the linear correction assumption is valid in the particle size range of interest, we would expect that the ERI we retrieve would be close to 1.585. The approximate solution for ERI during the PSL experiment was ranging from 1.57 to 1.6, which is close to the target value of 1.585. Therefore, we conclude that the OPC sizing error in the particle size range we are interested in, is corrected by applying a constant amplitude factor.

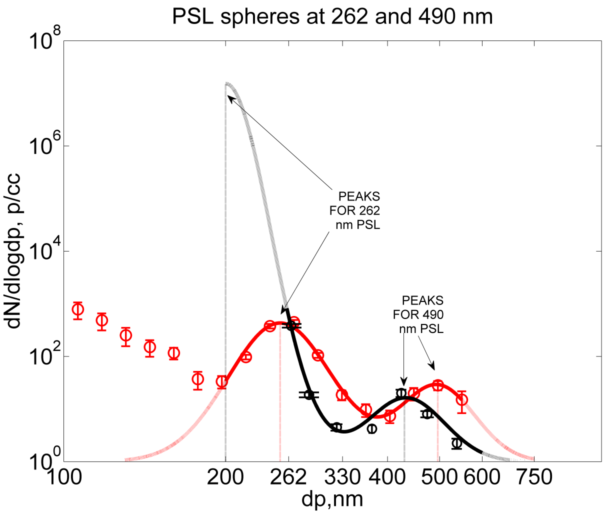

Figure S2: Calibration of SMPS-OPC ERI with PSL spheres at 262 and 490 nm. Red circles correspond to SMPS average concentration during the PSL experiment. Error bars correspond to the standard deviation from the average of each bin, for all size distributions measured during the experiment. Red line corresponds to SMPS lognormal distributions identified for the PSL sizes. Intense red color corresponds to the part of the lognormal distribution based on measurements, while the fade red line corresponds to the extended part of the distribution. The black circles, error bars and line correspond to the OPC. We observe that while SMPS sizes PSL correctly at 490 nm, OPC has a peak concentration at 430 nm size bin.

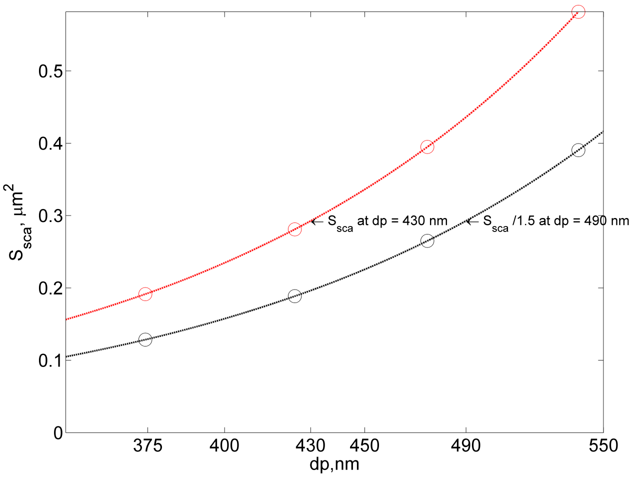

Figure S3: S_{sca} values versus homogeneous aerosol particle diameter dp for the OPC geometry and RI = 1.585. Theoretical scattering intensity according to equation 2 multiplied by particle cross section (red line); idem, as previously, divided by 1.5 (blue line); We observe that the theoretically predicted S_{sca}, when we apply this factor, can approach the experimentally determined one, within the particle size range we are interested in.

S_{sca} has to be corrected in the ERI retrieval algorithm according to equation S1.

$$S_{sca-cor} = \frac{S_{sca}}{1.5} \quad \text{(S1)}$$

The next step is to find a correction factor for aerosols with different RI. The final ERI correction equation for the sizing error and their dependence on aerosol RI follows:

$$RI = 1.7 * \exp((-(ERI_{COR} - 2)/1.5)^2) \quad \text{(S2)}$$

The next step is to evaluate if the above mentioned corrections can be applied to aerosols with different RI.

Figure S4 displays the calibration of SMPS-OPC derived ERI with dried generated test aerosol, ERI to Literature RI (RI) for common pure compounds characteristic for atmospheric aerosol. There is good correlation between the ERI calculated and the RI of each substance. The median values for each calibration experiment are shown in red diamonds. DEHS calibration has 10 5-minute points while Ammonium Sulfate 15 and PSL more than 20. The black line displayed is the fit of all data points for the 3 calibration experiments.

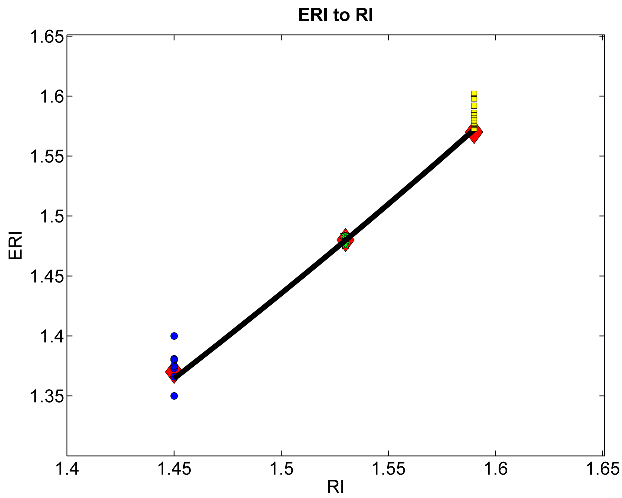

Figure S4: Best fit (black line) ERI to RI values for the calibration of SMPS-OPC with generated aerosol. Blue spots denote the 5-minute data points for the DEHS Experiment; green spots denote the 5-minute data points for the Ammonium Sulfate Experiment; yellow rectangles denote the 5-minute data points for the PSL Experiment; red diamonds denote the median value for each experiment.

Table S1: Literature RI (RI) versus ERI median values (MED ERI). Standard deviation (STDEV ERI), regression analysis R-squared and standard error (STD ERROR) are also presented.

PARAMETER	DEHS	AMMONIUM SULFATE	PSL SPHERES Diameter = 490 nm
RI	1.45	1.53	1.585
MED ERI	1.37	1.48	1.57
STDEV ERI	0.02	0.01	0.01
R-squared	0.98		
STD ERROR	0.1		

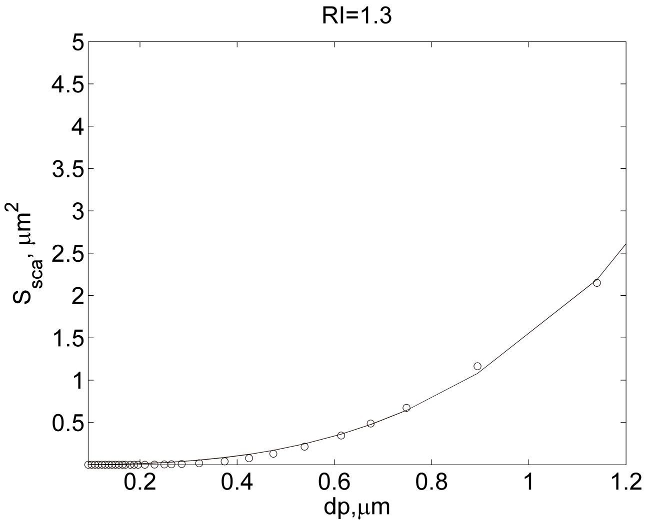

Figure S5: Best fit of S_{sca} at OPC diameter range for RI = 1.3.

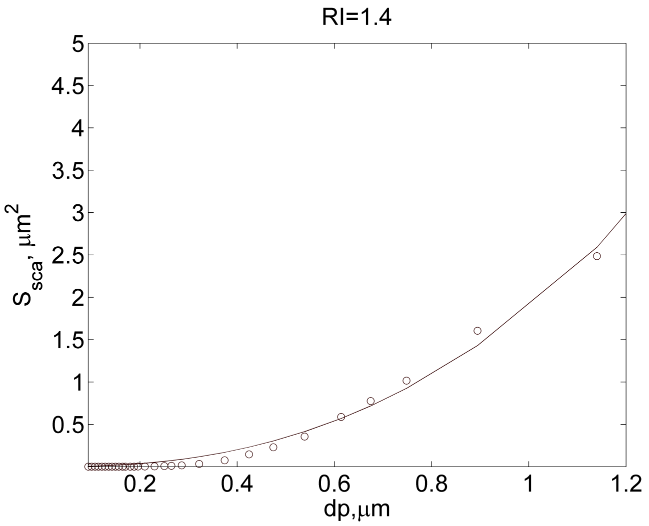

Figure S6: Best fit of S_{sca} at OPC diameter range for RI = 1.4.

In Table S1 we present the results of the calibration experiments. We observe that ERI underestimates RI for ammonium sulfate and DEHS, while it overestimates RI for PSL. Nevertheless, R-squared is close to 1 for all experiments, and the standard error is 0.1. Therefore we conclude that there is a good correlation between ERI and RI for these measurements.

Supplementary: Scattering effective cross section to diameters in the OPC size range and below

Figures S5-S10.

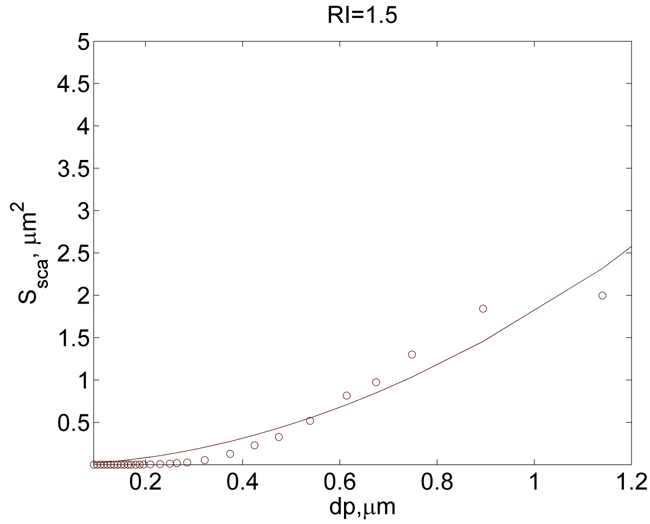

Figure S7: Best fit of S_{sca} at OPC diameter range for RI = 1.5.

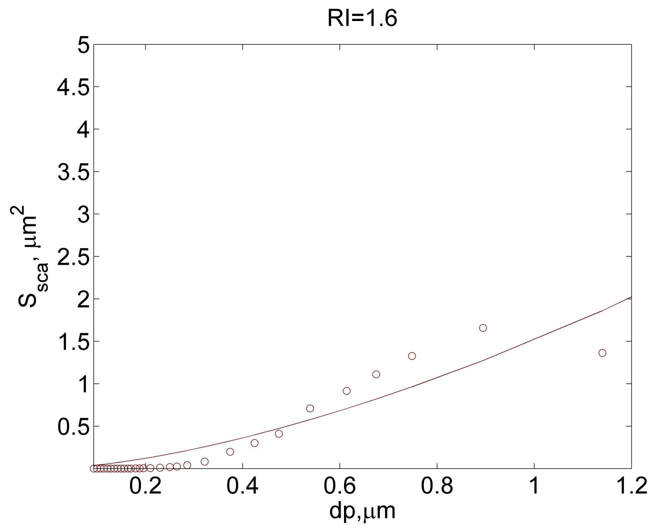

Figure S8: Best fit of S_{sca} at OPC diameter range for RI = 1.6.

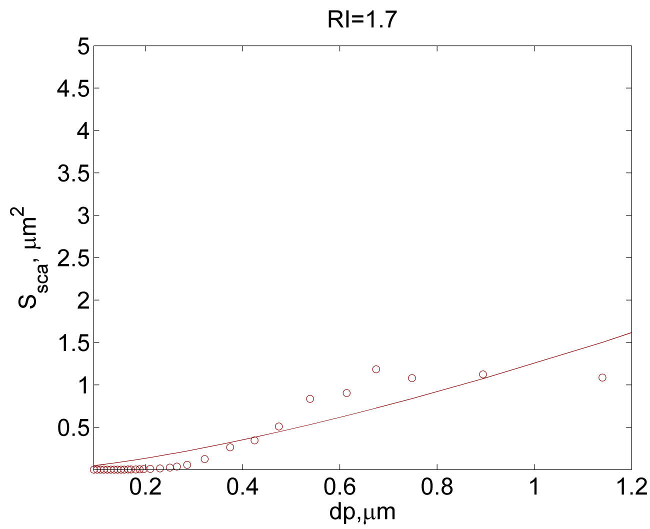

Figure S9: Best fit of S_{sca} at OPC diameter range for RI = 1.7.

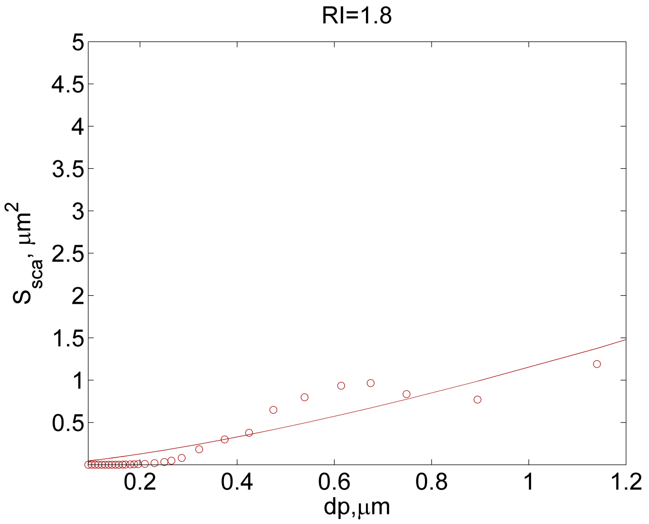

Figure S10: Best fit of S_{sca} at OPC diameter range for RI = 1.8.

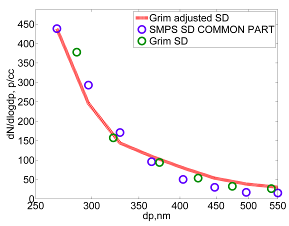

(a) SMPS - OPC FIT, ERI = 1.8

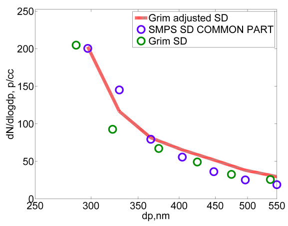

(b) SMPS - OPC FIT, ERI = 1.7

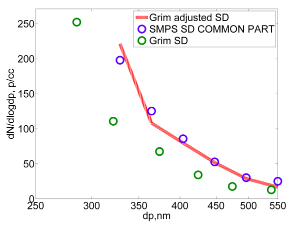

(c) SMPS - OPC FIT, ERI = 1.6

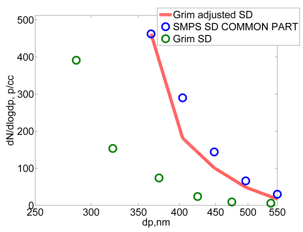

(d) SMPS - OPC FIT, ERI = 1.5

Figure S11: SMPS - OPC fit examples for various ERI values. Green circles denote the measured OPC size distribution (NSD), blue circles denote the SMPS NSD, while the red line represents the OPC, adjusted NSD. We observe that the final adjusted Grim OPC size distribution (SD) is very close to the SMPS NSD. Also, the OPC NSD at 430 nm is moved to the right to 490 nm at ERI = 1.6, as it should, in order to compensate for the sizing error in relation to the SMPS observed at the PSL calibration experiment.

Supplementary: SMPS-OPC FIT in the overlapping range

Figure S11.

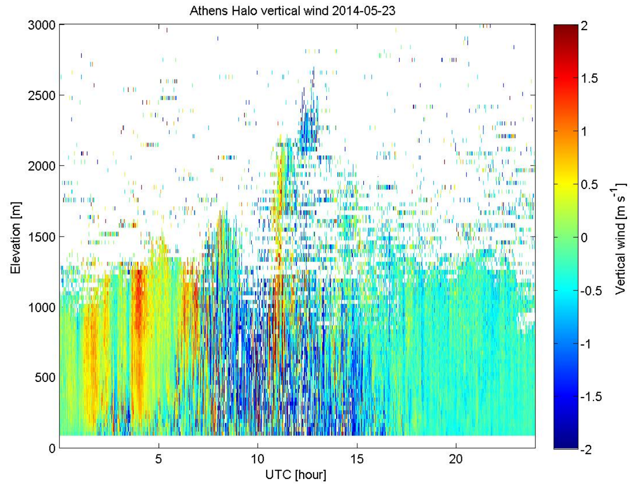

Figure S12: We observe that from 8:30 to 13:30 (IC filter measurement hours) there is strong mixing in the vertical, leading dust to DEM station. RI_{LI} was also calculated for this day (19:00-20:00 UTC).

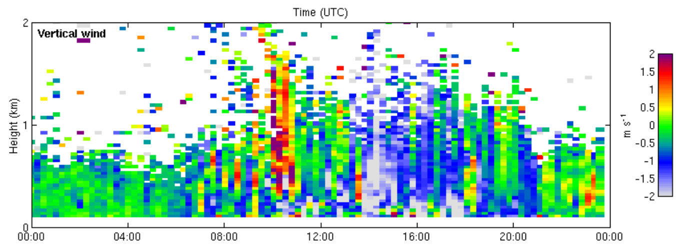

Figure S13: We observe that from 8:30 to 13:30 (IC filter measurement hours) there is strong mixing in the vertical, leading dust to DEM station.

Supplementary: HALO lidar vertical wind for days that the hypothesis of uniform dust concentration during the day does not hold

In the calculation of RI_{IC}, the 24h average of dust concentration (calculated from XRF measuments) was used. The hypothesis was that dust concentration during the day was closely following the concentration of other aerosol constituents. This does not hold for days that exhibit strong mixing in the vertical during the filter measurements and less mixing the rest of the day, while a Sahara dust event is occurring. ERI_{COR} calculated for the hours corresponding to RI_{IC}, is significantly higher during these days, as expected. (Figures S12-S13).

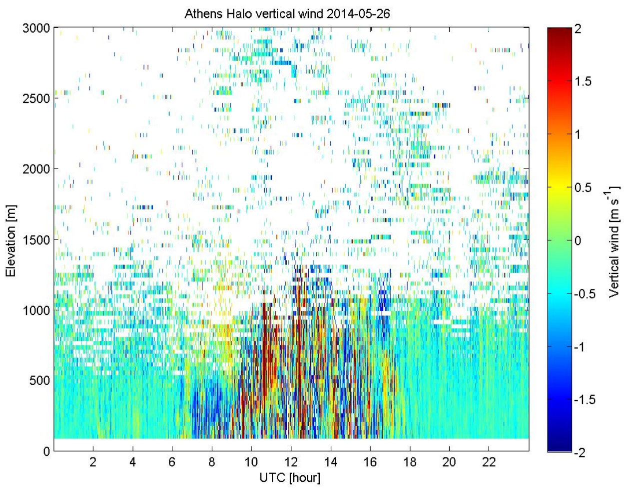

Figure S14: We observe that from 19:00-20:00 there is strong mixing in the vertical.

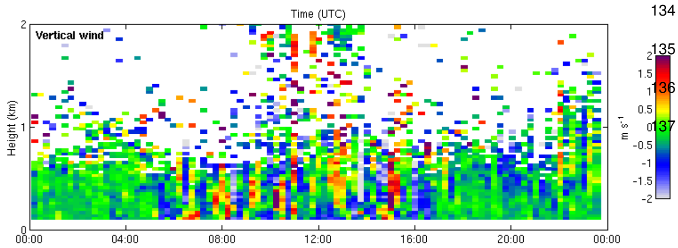

Figure S15: We observe that from 22:00-23:00 there is strong mixing in the vertical.

Supplementary: HALO lidar vertical wind for days that RI_{LI} was calculated

Figures S14-S16

On 17th of June 2014, 19:00-20:00, and 18th of June 2014, 19:00-20:00, the boundary layer heights are approximately 1.1 km and 1.0 km respectively, according to ECMWF ERA-INTERIM data.

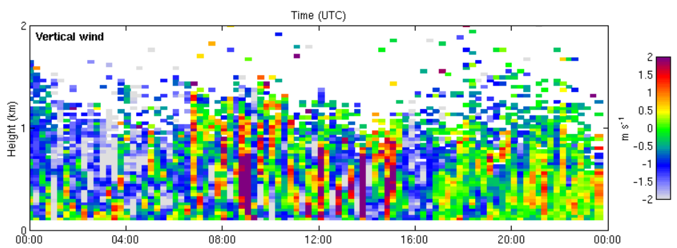

Figure S16: We observe that from 18:45-19:45 there is strong mixing in the vertical.

Table S2: Comparison of lidar derived RI values (RI_{LI}) to ERI_{COR} values obtained by SMPS-OPC (7 different days).

Date, Time (UTC)	ERI_{COR}	RI_{LI}
23th of May 2014, 19:00-20:00	1.61±0.1	1.56±0.1
26th of May 2014, 19:00-20:00	1.63±0.1	1.6±0.1
7th of June 2014, 22:00-23:00	1.67± 0.1	1.61±0.1
10th of June 2014, 18:45-19:45	1.68±0.1	1.62±0.1
17th of June 2014, 19:00-20:00	1.66±0.1	1.59±0.1
18th of June 2014, 19:00-20:00	1.58±0.1	1.59±0.1
22nd of June 2014, 19:00-20:00	1.6±0.1	1.56±0.1

Supplementary: RI_{LI} and ERI_{COR} availiable values

The availiable values for RI_{LI} and ERI_{COR} are presented in Table S2. In Figure 6, the value corresponding to the 22nd of June is not included, because RH was not availiable for that day.